

See discussions, stats, and author profiles for this publication at: <https://www.researchgate.net/publication/51199531>

# Trypanosomal Dihydrofolate Reductase Reveals Natural Antifolate Resistance

ARTICLE in ACS CHEMICAL BIOLOGY · JUNE 2011

Impact Factor: 5.33 · DOI: 10.1021/cb200124r · Source: PubMed

---

CITATIONS

9

READS

58

## 7 AUTHORS, INCLUDING:



Jarunee Vanichtanankul

National Center for Genetic Engineering and ...

19 PUBLICATIONS 634 CITATIONS

[SEE PROFILE](#)



Jirundon Yuvaniyama

Mahidol University

31 PUBLICATIONS 868 CITATIONS

[SEE PROFILE](#)



Tirayut Vilaivan

Chulalongkorn University

116 PUBLICATIONS 1,978 CITATIONS

[SEE PROFILE](#)



Yongyuth Yuthavong

National Center for Genetic Engineering and ...

174 PUBLICATIONS 3,991 CITATIONS

[SEE PROFILE](#)

# Trypanosomal Dihydrofolate Reductase Reveals Natural Antifolate Resistance

Jarunee Vanichtanankul,<sup>†,‡</sup> Supannee Taweechai,<sup>†</sup> Jirundon Yuvaniyama,<sup>‡</sup> Tirayut Vilaivan,<sup>§</sup> Penchit Chitnumsub,<sup>†</sup> Sumalee Kamchonwongpaisan,<sup>†</sup> and Yongyuth Yuthavong<sup>\*,†</sup>

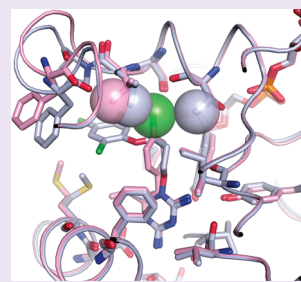
<sup>†</sup>National Center for Genetic Engineering and Biotechnology, National Science and Technology Development Agency, 113 Thailand Science Park, Paholyothin Road, Klong Luang, Pathumthani 12120, Thailand

<sup>‡</sup>Department of Biochemistry and Center for Excellence in Protein Structure and Function, Faculty of Science, Mahidol University, Rama 6 Road, Bangkok 10400, Thailand

<sup>§</sup>Department of Chemistry, Faculty of Science, Chulalongkorn University, Bangkok 10330, Thailand

Supporting Information

**ABSTRACT:** Dihydrofolate reductase (DHFR) is a potential drug target for *Trypanosoma brucei*, a human parasite, which is the causative agent for African sleeping sickness. No drug is available against this target, since none of the classical antifolates such as pyrimethamine (PYR), cycloguanil, or trimethoprim are effective as selective inhibitors of *T. brucei* DHFR (TbDHFR). In order to design effective drugs that target TbDHFR, co-crystal structures with bound antifolates were studied. On comparison with malarial *Plasmodium falciparum* DHFR (PfDHFR), the co-crystal structures of wild-type TbDHFR reveal greater structural similarities to a mutant PfDHFR causing antifolate resistance than the wild-type enzyme. TbDHFR imposes steric hindrance for rigid inhibitors like PYR around Thr86, which is equivalent to Ser108Asn of the malarial enzymes. In addition, a missing residue on TbDHFR active-site loop together with the presence of Ile51 widens its active site even further than the structural effect of Asn51Ile, which is observed in PfDHFR structures. The structural similarities are paralleled by the similarly poor affinities of the trypanosomal enzyme for rigid inhibitors. Mutations of TbDHFR at Thr86 resulted in 10-fold enhancement or 7-fold reduction in the rigid inhibitors affinities for Thr86Ser or Thr86Asn, respectively. The co-crystal structure of TbDHFR with a flexible antifolate WR99210 suggests that its greater affinity result from its ability to avoid such Thr86 clash and occupy the widened binding space similarly to what is observed in the PfDHFR structures. Natural resistance to antifolates of TbDHFR can therefore be explained, and potential antifolate chemotherapy of trypanosomiasis should be possible taking this into account.



Trypanosomal infections, including sleeping sickness caused by *Trypanosoma brucei*, threaten over 60 million people in 36 countries of sub-Saharan Africa and lack an optimal therapeutic treatment.<sup>1,2</sup> Current therapeutic regimens target either the hemolymphatic phase or neurological stage. These treatments have been used for more than 50 years with poor efficacy and complication of drug toxicity. For the neurological stage, various combinations of melarsoprol, eflornithine, and nifurtimox have been tested.<sup>3</sup> An efficient treatment recommended by WHO is the combination of oral nifurtimox and infusion of eflornithine.<sup>4</sup> Nevertheless, problems including difficulty of application and undesirable side effects are still unresolved. There is an urgent need for the development of new effective drugs against the protozoa.

Antifolate chemotherapy, through inhibition of the enzyme dihydrofolate reductase (DHFR), offers a potential treatment. Although *Trypanosoma* spp. and other Kinetoplastids have an alternative enzyme, pteridine reductase 1 (PTR1), which can reduce dihydrofolate in addition to DHFR,<sup>5</sup> its activity is not sufficient to compensate for the loss of DHFR activity, supporting the value of DHFR as an antitrypanosomal target.<sup>6</sup> While most clinically used DHFR inhibitors such as pyrimethamine

(PYR), cycloguanil, and trimethoprim show only poor activities, other experimental ones have been shown to be effective against leishmania and trypanosomes.<sup>7–11</sup> Some DHFR inhibitors have been also successful in the treatment of toxoplasmosis, as well as holding promise against cryptosporidiosis.<sup>12</sup> Furthermore, potent inhibitors of both trypanosomal PTR1 and DHFR have shown good antitrypanosomal activity.<sup>13</sup>

The structure of *T. brucei* DHFR (TbDHFR) should provide a good template for design of effective antifolate antitrypanosomal inhibitors, such as those against other DHFRs. For such design to be successful, it is important to know whether the TbDHFR active site is similar to other protozoal DHFRs. In particular, because the structures of both wild-type or PYR-resistant mutant *Plasmodium falciparum* DHFR (PfDHFR) are known<sup>14</sup> and have provided explanation for the resistance, a comparison with TbDHFR may provide important clues to effective drug design. Herein, we report the first crystal structures of wild-type TbDHFR, in ternary

**Received:** April 20, 2011

**Accepted:** June 8, 2011

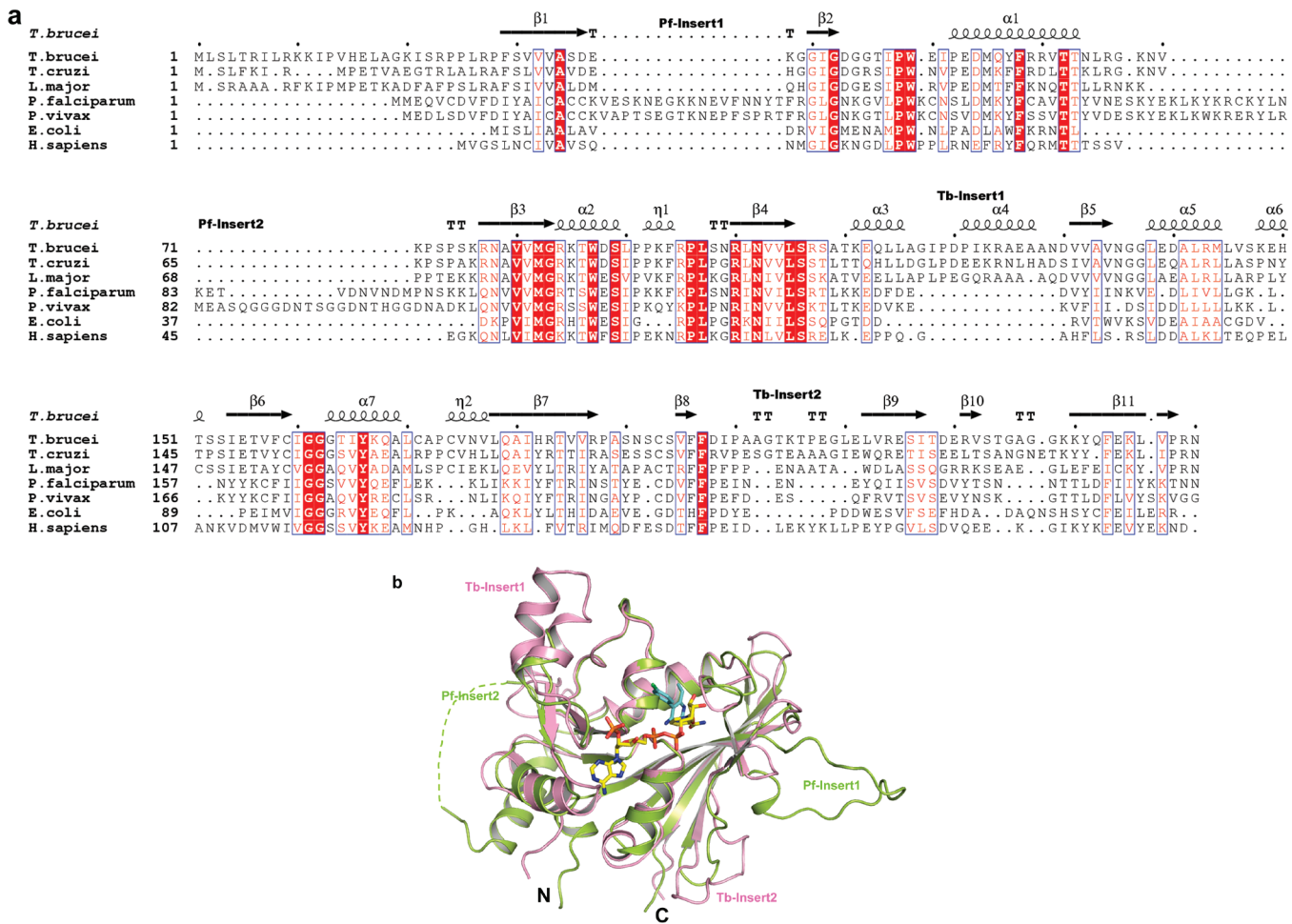


**Figure 1.** Structure-based alignment of DHFR and structural comparison of TbDHFR and PfDHFR. (a) Alignment is based on pairwise structure superposition in program O using TbDHFR as a reference structure with minor manual adjustment. Insert sequences Pf-Insert1 (residues 20–36) and Pf-Insert2 (residues 64–99) of *P. falciparum*, as well as Tb-Insert1 (residues 117–129) and Tb-Insert2 (residues 202–210) of *T. brucei*, are labeled. Secondary structure of TbDHFR is assigned and shown with arrows and helical features representing  $\beta$ -stands and  $\alpha$ -helices, respectively. Strictly conserved residues are highlighted in red with white characters, and similar residues within a group are in blue frames with red characters. (b) Superposition of TbDHFR (pink) in complex with NADPH (yellow) and PYR (cyan) to PfDHFR-TM4 (green) presents different topographic point of inserts.

complexes with NADPH and PYR or WR99210, and compare them with wild-type (TM4) and Asn51Ile + Cys59Arg + Ser108-Asn + Ile164Leu quadruple mutant (V1/S) PfDHFR-thymidylate synthase (PfDHFR-TS). Kinetics and inhibition properties of wild-type and mutant TbDHFRs are also presented. Together, these findings provide important insight for potential antifolate chemotherapy of trypanosomiasis.

## ■ RESULTS AND DISCUSSION

**Overall Structure of *T. brucei* DHFR.** Although various attempts to obtain crystals of the bifunctional TbDHFR-TS for X-ray structure determination have been unsuccessful, we could crystallize the TbDHFR domain, consisting of residues 24–242, and obtain its structure at 2.0 Å resolution. This contains 11 β-strands, seven α-helices, and two 3<sub>10</sub> helices (Figure 1, panel a). Despite similarity in the overall structures of TbDHFR and DHFR domains of the homodimeric, bifunctional DHFR-TS of other Kinetoplastids such as *Leishmania major*<sup>15</sup> and *T. cruzi*<sup>16,17</sup> and of Apicomplexans like *Cryptosporidium hominis*<sup>18</sup> and *P. falciparum*,<sup>14</sup> different insert sequences are observed at various

positions on the surface of the core structure (Figure 1, panel b). DHFR-TS of Apicomplexans have an elongated junction region between the DHFR and TS domains, while those of the Kinetoplastids contain extended a N-terminus that embraces the TS domain as seen in *L. major* and *T. cruzi* DHFR-TS,<sup>15–17</sup> providing different interdomain arrangement and contacts. While Pf-Insert1 (residues 20–36) provides anchoring interactions of PfDHFR with the PfTS domains,<sup>14</sup> Tb-Insert1 (residues 117–129) and Tb-Insert2 (residues 202–210) are found to interact with symmetry-related molecules and thus stabilize the crystal contacts. The regions equivalent to those Tb inserts in *L. major* DHFR-TS are disordered and therefore not involved in interdomain stabilization.<sup>15</sup>

**Active-Site Comparison with *P. falciparum* DHFR.** Comparison of active-site structures among the ternary complexes of TbDHFR, PYR-sensitive (TM4), and PYR-resistance (V1/S) PfDHFRs indicates that there is steric conflict in the binding of PYR to TbDHFR and V1/S. Using the binding mode of PYR to TM4 as a reference, the longer side chain of Asn108 of V1/S results in steric clash with PYR and NADPH as shown by a slight tilt of the phenyl ring of PYR and a 42° twist of the nicotinamide

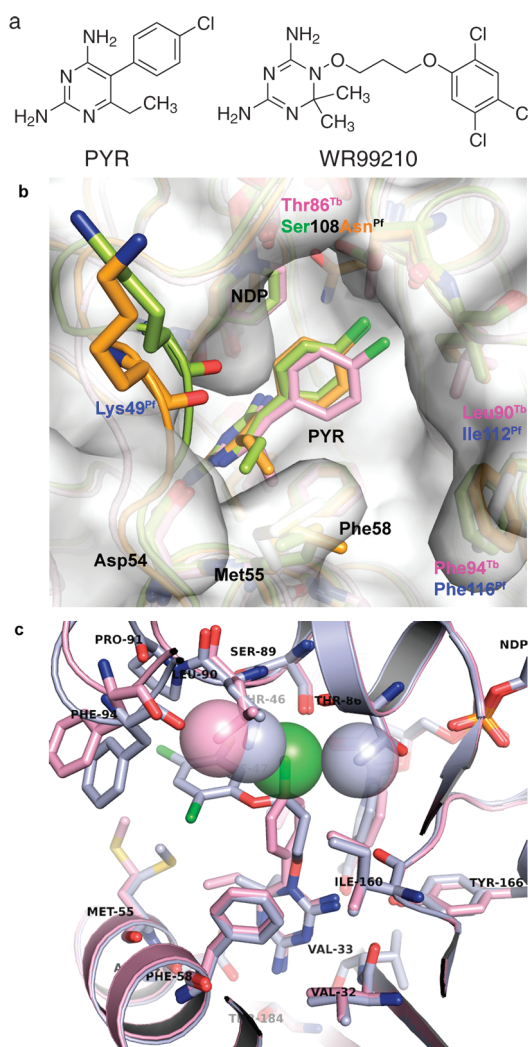


**Figure 2.** Classical antifolates and active site comparison of PfDHFR and TbDHFR. (a) Structure of Pyrimethamine (PYR) and WR99210 are rigid and flexible inhibitor, respectively. (b) Superposition of the ternary complexes of TbDHFR (pink), PfDHFR-TM4 (green), and PfDHFR-V1/S (orange) drawn with TbDHFR molecular surface displays a displacement of PYR and wider active-site opening in TbDHFR. Key residues are labeled in the corresponding colors of the models shown, except common residues between TbDHFR and PfDHFR are labeled in black and residues for PfDHFRs are labeled in blue. PfDHFR Lys49 is absent in TbDHFR. (c) WR99210 (light blue) fits snugly in the active-site pocket of TbDHFR, whereas the chlorine atom (green) of PYR (pink) sterically clashes with C $\gamma$  atom of Thr86 and C $\delta$  atom of Leu90 (shown with spheres). The side chains of residues within 3.5 Å around the ligands are shown. Oxygen, nitrogen, phosphorus, sulfur, and chlorine atoms are colored red, blue, orange, yellow, and green, respectively.

ring of its bound NADPH (Figure 2, panel b) with poorer electron density for the ring as compared with the rest of the NADPH (data not shown). This steric conflict is likely the cause of PYR resistance as seen in Cys59Arg + Ser108Asn double mutant K1CB1 PfDHFR-TS.<sup>14</sup> Despite the similar side-chain lengths of Ser108 of TM4 and the corresponding Thr86 residue of TbDHFR, the extra methyl group on Thr86 pushes against the p-Cl-phenyl group of PYR, causing a displacement of the rigid antifolate PYR at its chlorine atom by 1.2 Å in comparison with

both wild-type TM4 and mutant V1/S (Figure 2, panel b). This situation is similar to that for *P. vivax* DHFR, in which the Cl atom of PYR bound to SP21 (Ser58Arg + Ser117Asn) mutant enzyme is also displaced by 1.1 Å from its position in the complex with the wild-type enzyme.<sup>19</sup> In addition, the shifted p-Cl-phenyl group of PYR in TbDHFR is pushed against the side chain of Leu90, causing movements of the C $\delta$  atom of Leu90 by 1.4 Å and the loop containing residues Pro91–Phe94 by up to 2.3 Å in comparison with WR99210 complex structure (Figure 2, panel c). Unlike rigid compounds, flexible antifolates such as WR99210 bound to TbDHFR structure could avoid such steric clashes by bending along the active-site pocket (Figure 2, panel c) in a similar conformation as observed in PfDHFRs<sup>14</sup> and thus bind more tightly than rigid inhibitors, as shown by the 232-fold higher  $K_i$  value for cycloguanil (CYC) and the 22-fold higher result for PYR (Table 1). Furthermore, one of the two methyl groups of CYC has van der Waals repulsion to the C $\beta$  atom of Ala34 and C $\delta$  atom of Ile47 (data not shown), equivalent to Ala16 and Leu46 of PfDHFR, which leads to a 10-fold higher  $K_i$  value compared with that of PYR. However, the fact that PfDHFR with Ser108Thr mutation is sensitive to both PYR and CYC<sup>20</sup> indicates that the reduced affinity of PYR to TbDHFR active site involve additional factors.

Another notable similarity between TbDHFR and V1/S PfDHFR can be drawn from the fact that the latter has a widened active-site opening as compared with TM4 due to substantial outward shift of residues 48–51 of V1/S PfDHFR, a part of the Leu46 loop covering the active-site pocket, and a minor displacement of residues 164–167.<sup>14</sup> This Leu46 loop is likely equivalent to the Met20 loop of *Escherichia coli* DHFR, which facilitates ligand binding and release through adoption of different conformations during the catalytic cycle.<sup>21</sup> Compared with V1/S PfDHFR, TbDHFR also has a similarly wide active-site entrance, due principally to an absence of a residue equivalent to Lys49 of PfDHFR (Figure 2, panel b). Strikingly, the native sequence of TbDHFR contains Ile51 and Arg59, which are equivalent to Asn51Ile and Cys59Arg mutation sites of V1/S PfDHFR, respectively. Ile51, which is located at the end of the TbDHFR Ile47 loop equivalent to the Leu46 loop of PfDHFR, is also associated with the same structural conformation as Ile51 in V1/S PfDHFR, contributing to the wide active-site opening as reported for the latter<sup>14</sup> (Figure 2, panel b). Moreover, Arg59 of TbDHFR is expected to mimic the rescuing role of Arg59 of PfDHFR from the V1/S mutant, offering additional ionic attraction with the glutamate moiety of the DHF substrate in the surroundings of antifolate-resistant mutations.<sup>14</sup> Altogether, the active site of native TbDHFR is therefore more similar to mutant PfDHFRs associated with antifolate resistance than the wild-type enzyme.

**Natural Antifolate Resistance Confirmed by Site-Specific Mutations.** Our hypothesis that TbDHFR would interact with inhibitors similarly to PfDHFR associated with PYR resistance (V1/S) and differently from PYR-sensitive TM4 PfDHFR is borne out by enzyme inhibition studies. TbDHFR displays substantially higher inhibition constant ( $K_i$ ) values for rigid antifolate inhibitors, including PYR and CYC, than TM4 PfDHFR, similarly to V1/S PfDHFR (Figure 3, panel a and Supplementary Table S1). Flexible inhibitors such as WR99210, which remain effective with mutant PfDHFRs by virtue of its ability to adopt a conformation that optimizes interaction with the changed active site, were found also to be effective against TbDHFR (Figure 3, panel b and Supplementary Table S2). In

**Table 1.** Kinetic Parameters and Binding Affinity of Wild-Type and Mutants of TbDHFR

constructs of TbDHFR	kinetic parameters				$K_i$ value (nM)		
	$k_{cat}$ ( $s^{-1}$ )	$K_m^{DHF}$ ( $\mu M$ )	$K_m^{NADPH}$ ( $\mu M$ )	$k_{cat}/K_m^{DHF}$ ( $s^{-1} \mu M^{-1}$ )	PYR	CYC	WR99210
wild-type	$3.11 \pm 0.17$	$3.85 \pm 0.19$	$4.43 \pm 0.36$	0.81	$24.2 \pm 1.3$	$256 \pm 7.4$	$1.1 \pm 0.3$
Thr86Ser	$4.54 \pm 0.33$	$16.25 \pm 3.14$	$7.92 \pm 0.23$	0.28	$2.1 \pm 0.1$	$20.5 \pm 0.8$	$0.9 \pm 0.1$
Thr86Asn	$3.75 \pm 0.25$	$30.51 \pm 6.31$	$5.23 \pm 0.60$	0.12	$179 \pm 49$	$1915 \pm 498$	$3.9 \pm 0.4$

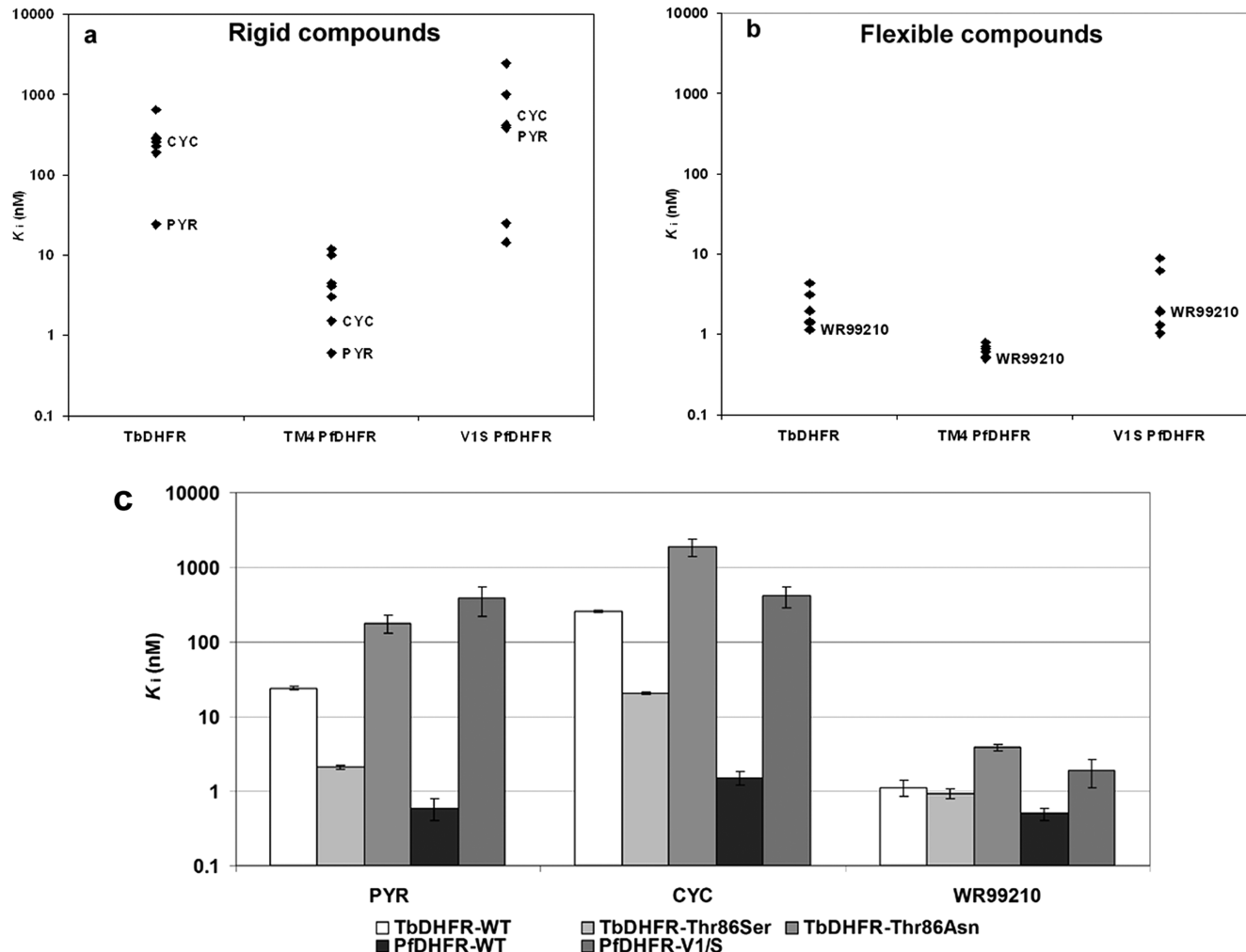


**Figure 3.** Inhibition constants against TbDHFRs and PfDHFRs of rigid and flexible antifolates.  $K_i$  values of (a) rigid and (b) flexible analogues of 4,6-diamino-1,2-dihydro-1,3,5-triazine are shown with the reference values of pyrimethamine (PYR), cycloguanil (CYC), and WR99210. (c)  $K_i$  values of classical antifolates with wild-type and mutant forms of TbDHFR and PfDHFR indicate influence of Thr86Ser and Thr86Asn for TbDHFR. The plot shows the average values from at least three experiments, and the error bars indicate the standard deviations.

order to verify our prediction further, mutants of TbDHFR were created that would mimic wild-type PfDHFR (Thr86Ser TbDHFR) or further resemble mutant PfDHFRs associated with drug resistance (Thr86Asn TbDHFR). The Thr86Ser and Thr86Asn TbDHFRs have 4- and 9-fold lower catalytic activities than the wild-type enzyme, respectively. The  $K_i$  values of PYR and CYC against Thr86Ser TbDHFR are decreased by 1 order of magnitude, while those against Thr86Asn TbDHFR are higher by a factor of 7 as expected (Table 1 and Figure 3, panel c).

**Implications for Antitrypanosomal Drug Design.** The promise of TbDHFR inhibitors as antitrypanosomal agents is revealed from the fact that *T. brucei* in culture is inhibited by a

number of antifolates.<sup>7–11,13</sup> Our structural data of TbDHFR, which is supported by the  $K_i$  values for various inhibitors, together with data from recombinant TbDHFR mutants prove the hypothesis that the TbDHFR is similar to mutant PfDHFRs associated with PYR resistance. This is also consistent with data on cytotoxic effect of WR99210 against *T. brucei* in culture with the IC<sub>50</sub> value of  $0.09 \pm 0.02 \mu M$  despite inactivity of PYR and CYC up to  $25 \mu M$ . This conclusion has implications for development of antitrypanosomal drugs that target DHFR. In light of the fact that new PfDHFR inhibitors are being developed to combat PYR-resistant malarial parasites,<sup>22</sup> the search for effective trypanosomal DHFR inhibitors should benefit from such development.

**Table 2. Data Collection and Refinement Statistics**

	TbDHFR–NADPH–WR99210	TbDHFR–NADPH–PYR	TM4 PfDHFR-TS–NADPH–PYR	V1/S PfDHFR-TS–NADPH–PYR
Data Collection				
space group	<i>P</i> 4 <sub>1</sub>	<i>P</i> 4 <sub>1</sub>	<i>P</i> 2 <sub>1</sub> 2 <sub>1</sub> 2 <sub>1</sub>	<i>P</i> 2 <sub>1</sub> 2 <sub>1</sub> 2 <sub>1</sub>
cell dimensions (Å)				
<i>a</i>	58.409	58.239	56.096	56.486
<i>b</i>	58.409	58.239	154.436	155.272
<i>c</i>	151.123	149.142	164.005	164.995
resolution <sup>a</sup> (Å)	50–2.0 (2.07–2.0)	50–2.20 (2.28–2.20)	50–2.30 (2.38–2.30)	50–2.20 (2.28–2.20)
<i>R</i> <sub>merge</sub> <sup>a</sup> (%)	5.5 (22.9)	7.3 (38.6)	8.2 (46.8)	8.8 (54.2)
< <i>I</i> / <i>σI</i> > <sup>a</sup>	23.1 (5.2)	21.8 (4.3)	16.0 (2.3)	15.7 (2.2)
completeness <sup>a</sup> (%)	98.8 (90.5)	100 (99.8)	99.3 (96.0)	99.1 (91.6)
redundancy	4.4	7.2	4.6	6.1
Refinement				
resolution (Å)	50–2.0	50–2.2	50–2.3	50–2.3
no. reflections (unique)	33,582	25,132	63,588	65,378
<i>R</i> <sub>work</sub> / <i>R</i> <sub>free</sub> <sup>b</sup>	18.3/22.1	18.7/23.5	21.8/25.5	19.8/23.3
av <i>B</i> -factors of enzyme (Å <sup>2</sup> )	25.1	29.2	44.0	41.1
no. atoms				
protein	3,330	3,323	9,044	9,058
NADPH	96	96	96	96
WR99210/PYR	48	34	34	34
dUMP	—	—	40	40
water	512	343	319	529
Ramachandran plot (non-Gly and non-Pro residues)				
most favored regions	333 (92%)	339 (93.1%)	851 (85.5%)	855 (85.9%)
additional allowed regions	29 (8%)	25 (6.9%)	139 (14%)	139 (14%)
generously allowed regions	0	0	3 (0.3%)	1 (0.1%)
disallowed regions	0	0	2 <sup>c</sup> (0.2%)	0
rms deviation				
bond lengths (Å)	0.006	0.006	0.007	0.006
bond angles (deg)	1.8	1.7	1.4	1.4

<sup>a</sup>Values in parentheses are for the highest-resolution shell. <sup>b</sup>*R*<sub>free</sub> is calculated from 5% of reflections chosen randomly in each of the 10 resolution bins.

<sup>c</sup>Two residues are Lys49, each located on a flexible loop of each of PfDHFR-TS two subunits.

## METHODS

**Cloning of Tbdhfr-ts and Tbdhfr.** *Tbdhfr-ts* and *Tbdhfr* genes were PCR-amplified from genomic DNA of *T. brucei rhodesiense* parasite (generously provided by V. Yardley from London School of Hygiene and Tropical Medicine, U.K.) using a forward primer with *Sac*I site in italic, 5'-CTC GAG CTC ATG CTC AGT CTT ACG CGT ATC-3', and the reverse primers with *Eco*RI site, 5'-CCG GAA TTC CTA CAC CGC CAT CTC CAT-3' and 5'-CCG GAA TTC CTA TTC GCT GTT TCG GGG G-3' for *Tbdhfr-ts* and *Tbdhfr* genes, respectively. The PCR protocol was initiated at 95 °C for 5 min, followed by 30 cycles of 1 min at 95 °C, 1 min at 53 °C, 2 min at 72 °C, and a final 10-min incubation at 72 °C. The amplified fragments of 1581 bp and 726 bp for *Tbdhfr-ts* and *Tbdhfr*, respectively were purified using QIAquick PCR Purification Kit and ligated into the sites of *Sac*I and *Eco*RI of the modified pET17b plasmid, in which the original *Nde*I site had been changed to *Sac*I. Following transformation of *E. coli* DH5α, positive clones with the insert genes were screened by PCR amplification from colonies grown on LB agar supplemented with 100 μg mL<sup>-1</sup> ampicillin. Plasmids from the positive clones were verified by DNA sequencing.

**Site-Directed Mutagenesis of Tbdhfr.** *Tbdhfr* gene was mutated using pET17b-*Tbdhfr* as the template. Two oligonucleotide

primers, 5'-GTT GTG ATG GGG CGG AAA AGT TGG GAC AGT CTT CCA CCA A-3' and 5'-TTG GTG GAA GAC TGT CCC A ACT TTT CCG CCC CAT CAC AAC-3' were used for Thr86Ser mutation with the codon of residue 86 underlined. Two oligonucleotide primers for Thr86Asn mutation were similarly designed with AAC and GTT replacing those underlined bases, respectively. The PCR protocol was initiated with 95 °C for 5 min, with subsequent 30 cycles of 95 °C for 1 min, 48 °C for 1 min, and 72 °C for 9 min. After elimination of DNA template by *Dpn*I digestion, the newly synthesized DNA was used to transform *E. coli* DH5α, and the cells were plated on LB agar containing 100 μg mL<sup>-1</sup> ampicillin. Colonies were grown in the presence of ampicillin for plasmid extraction and sequence verification by DNA sequencing.

**Expression and Purification of TbDHFR and PfDHFR-TS.** All wild-type and mutants of TbDHFR and PfDHFR-TS were expressed and purified using similar protocols described previously.<sup>23</sup> Briefly, clones containing DHFR or DHFR-TS gene were expressed in *E. coli* BL21 (DE3). Using 1.5% inoculum of an overnight culture, the cells were grown in LB broth containing 100 μg mL<sup>-1</sup> ampicillin at 37 °C until OD<sub>600</sub> was ~1.0. Protein expression was then induced with 0.4 mM of isopropyl β-D-thiogalactoside at 20 °C for 20 h. The overexpressed proteins were separately purified using a methotrexate-Sepharose column and eluted with dihydrofolate (DHF). The substrate DHF was removed by a HiPrep

26/10 desalting column (Amersham Bioscience). PfDHFR-TS proteins were further purified using a Q-Sepharose FF column (Amersham Bioscience). TbDHFR-TS protein expression from pET17b-*Tbdhfr-ts* yielded full-length TbDHFR-TS (59 kDa) and a truncated form of about 25–30 kDa with DHFR activity, similar to the result of a previous report.<sup>24</sup> Therefore, truncated TbDHFR enzyme was further purified by SP-Sepharose FF and Sephadryl S-200 HR (Amersham Bioscience) columns. Each protein was concentrated by ultrafiltration with 10 kDa MW cutoff (Amicon, Millipore). Protein concentrations were determined by Bradford assay using bovine serum albumin (BSA) as a standard.<sup>25</sup>

**Kinetic Analysis.** DHFR activities were determined spectrophotometrically at 340 nm by monitoring the consumption of NADPH using a reaction molar absorptivity of 12,300 M<sup>-1</sup> cm<sup>-1</sup>.<sup>22,26</sup> Briefly, 0.001–0.005 units of the purified enzyme was used in a 200  $\mu$ L reaction containing 50  $\mu$ M each of DHF and NADPH in 50 mM TES, pH 7.0, 75 mM  $\beta$ -mercaptoethanol, and 1 mg mL<sup>-1</sup> BSA. Compound libraries were obtained as previously described.<sup>22,27</sup> Inhibition constant ( $K_i$ ) was determined by measuring the inhibition of the DHFR activity at various inhibitor concentrations and fitting the data to nonlinear least-squares equation of competitive inhibitor using KaleidaGraph 3.51 (Synergy Software, Reading, PA).

**Cytotoxicity against *T. brucei rhodesiense* (*Tbr*) Trypomastigotes.** *Tbr* (STIB-900) trypomastigotes<sup>28,29</sup> were maintained in MEM/EBSS media supplemented with 25 mM HEPES, 4.5 g L<sup>-1</sup> glucose, 3.0 g L<sup>-1</sup> NaHCO<sub>3</sub>, 1% MEM non-essential amino acids, 0.2 mM 2-mercaptoethanol, 0.05 mM bathocuproinedisulphonic acid, 0.15 mM L-cysteine, 0.1 mM hypoxanthine, 1 mM sodium pyruvate, and 10% heated fetal bovine serum at 37 °C in a 3% CO<sub>2</sub> atmosphere with 95% humidity. To assay anti-*Tbr* activity, 100  $\mu$ L of 20,000 parasites with and without drug dilution was incubated for 69 h in a microplate. Alamar blue (20  $\mu$ L) was then added and incubated further for 3 h. The plate was read at excitation and emission wavelengths of 530 and 590 nm, respectively. The 50% inhibitory concentration (IC<sub>50</sub> value) was calculated against untreated control.

**Crystallization and Data collection.** The purified samples of TbDHFR (8 mg mL<sup>-1</sup>) and PfDHFR-TS (15 mg mL<sup>-1</sup>) were co-crystallized with the final concentration of 2 mM NADPH and 2 mM PYR or WR99210. The ternary complexes were crystallized using the microbatch method at 24 °C with the mixture of 1  $\mu$ L of protein complex and 1  $\mu$ L of crystallizing solution under baby oil (PZ Cussons, Ltd. Thailand).<sup>23,30</sup> The ternary complex of TbDHFR was crystallized in 0.05 M ammonium sulfate, 0.05 M bis-Tris, pH 6.5 and 32% (w/v) poly(ethylene glycol) 4000. Each of the single crystals was quickly transferred into cryoprotectant (20% glycerol in the crystallizing solution) for a few seconds and immediately vitrified in a stream of cold nitrogen (100 K). X-ray diffraction data were collected at Cu K $\alpha$  wavelength (1.5418 Å) on a Bruker-Nonius FR591 X-ray generator equipped with a  $\kappa$ CCD detector. Data were indexed, integrated and scaled using Denzo/Scalepack programs in HKL-2000 package.<sup>31</sup> Data processing statistics are shown in Table 2.

**Structure Determination and Refinement.** The TbDHFR structure was determined by the molecular replacement method using the structure of the DHFR domain of *L. major*<sup>15</sup> (with 47% identity to TbDHFR) as a search model with AMoRe<sup>32</sup> in the CCP4 Suite.<sup>33</sup> The Matthews' coefficient ( $V_M$ ) suggested two molecules in an asymmetric unit (ASU) with  $V_M$  of 2.3 Å<sup>3</sup> Da<sup>-1</sup> and 47% solvent content. The top solution was refined with rigid-body calculation and minimization. The Fourier difference ( $2F_o - F_c$  and  $F_o - F_c$ ) electron density maps were calculated using CNS<sup>34</sup> starting from 3 Å resolution. The model of TbDHFR was rebuilt using the program O.<sup>35</sup> The refinement in subsequent steps included minimization, simulated annealing, and individual  $B$  factor calculations with gradual extension to the highest resolution. The PfDHFR-TS TM4 and V1/S structures were determined through Fourier difference maps using PfDHFR-TS K1 (PDB id ij3j) as a template model.<sup>14</sup> The models were rebuilt using program O and refined

using CNS starting from 2.5 Å resolution gradually to the highest resolution. Ligands and water molecules were added to positive density of  $F_o - F_c$  map and verified in every cycle of the refinement.

The final models were verified with PROCHECK<sup>36</sup> and the final refinement statistics are shown in Table 2. Structural figures were prepared with PyMOL.<sup>37</sup> The sequence alignment with secondary structure of TbDHFR was prepared using ESPript 2.2.<sup>38</sup>

## ASSOCIATED CONTENT

**S Supporting Information.** This material is available free of charge via the Internet at <http://pubs.acs.org>.

## Accession Codes

Coordinates and structure factors have been deposited in the Protein Data Bank with the codes 3RG9 and 3QFX for the TbDHFR in complex with WR99210 and PYR, respectively. The PYR complexes of TM4 and V1/S PfDHFR-TS are listed as 3QGT and 3QG2, respectively.

## AUTHOR INFORMATION

### Corresponding Author

\*E-mail: yongyuth@biotec.or.th.

## ACKNOWLEDGMENT

We thank D.A. Matthews for *L. major* DHFR-TS coordinates and Miss Aunchalee Tonsomboon for technical assistance on anti-*Tbr* testing. This work was supported by Thailand Graduate Institute of Science and Technology (J.V. and S.T.), Synchrotron Light Research Institute (Public Organization), Thailand (P.C.), Thailand TDR Programme, and NSTDA Cluster and Program Management Office to the team. S.K. is an international scholar of Howard Hughes Medical Institute.

## REFERENCES

- (1) Fairlamb, A. H. (2003) Chemotherapy of human African trypanosomiasis: current and future prospects. *Trends Parasitol.* 19, 488–494.
- (2) Brun, R., Blum, J., Chappuis, F., and Burri, C. (2010) Human African trypanosomiasis. *Lancet* 375, 148–159.
- (3) Priotto, G., Fogg, C., Balasgaram, M., Erphas, O., Louga, A., Checchi, F., Ghabri, S., and Piola, P. (2006) Three drug combinations for late-stage *Trypanosoma brucei gambiense* sleeping sickness: a randomized clinical trial in Uganda. *PLoS Clin. Trials* 1, e39.
- (4) Opigo, J., and Woodrow, C. (2009) NECT trial: more than a small victory over sleeping sickness. *Lancet* 374, 7–9.
- (5) Nare, B., Hardy, L. W., and Beverley, S. M. (1997) The roles of pteridine reductase 1 and dihydrofolate reductase-thymidylate synthase in pteridine metabolism in the protozoan parasite *Leishmania major*. *J. Biol. Chem.* 272, 13883–13891.
- (6) Sienkiewicz, N., Jaroslawski, S., Wyllie, S., and Fairlamb, A. H. (2008) Chemical and genetic validation of dihydrofolate reductase-thymidylate synthase as a drug target in African trypanosomes. *Mol. Microbiol.* 69, 520–533.
- (7) Gilbert, I. H. (2002) Inhibitors of dihydrofolate reductase in *Leishmania* and trypanosomes. *Biochim. Biophys. Acta* 1587, 249–257.
- (8) Pez, D., Leal, I., Zuccotto, F., Boussard, C., Brun, R., Croft, S. L., Yardley, V., Ruiz Perez, L. M., Gonzalez Pacanowska, D., and Gilbert, I. H. (2003) 2,4-Diaminopyrimidines as inhibitors of leishmanial and trypanosomal dihydrofolate reductase. *Bioorg. Med. Chem.* 11, 4693–4711.
- (9) Khabnadideh, S., Pez, D., Musso, A., Brun, R., Perez, L. M., Gonzalez-Pacanowska, D., and Gilbert, I. H. (2005) Design, synthesis and evaluation of 2,4-diaminoquinazolines as inhibitors of trypanosomal and leishmanial dihydrofolate reductase. *Bioorg. Med. Chem.* 13, 2637–2649.

- (10) Zuccotto, F., Zvelebil, M., Brun, R., Chowdhury, S. F., Di Lucrezia, R., Leal, I., Maes, L., Ruiz-Perez, L. M., Gonzalez Pacanowska, D., and Gilbert, I. H. (2001) Novel inhibitors of *Trypanosoma cruzi* dihydrofolate reductase. *Eur. J. Med. Chem.* 36, 395–405.
- (11) Chowdhury, S. F., Villamor, V. B., Guerrero, R. H., Leal, I., Brun, R., Croft, S. L., Goodman, J. M., Maes, L., Ruiz-Perez, L. M., Pacanowska, D. G., and Gilbert, I. H. (1999) Design, synthesis, and evaluation of inhibitors of trypanosomal and leishmanial dihydrofolate reductase. *J. Med. Chem.* 42, 4300–4312.
- (12) Pelphrey, P. M., Popov, V. M., Joska, T. M., Beierlein, J. M., Bolstad, E. S., Fillingham, Y. A., Wright, D. L., and Anderson, A. C. (2007) Highly efficient ligands for dihydrofolate reductase from *Cryptosporidium hominis* and *Toxoplasma gondii* inspired by structural analysis. *J. Med. Chem.* 50, 940–950.
- (13) Cavazzuti, A., Paglietti, G., Hunter, W. N., Gamarro, F., Piras, S., Loriga, M., Allecca, S., Corona, P., McLuskey, K., Tulloch, L., Gibellini, F., Ferrari, S., and Costi, M. P. (2008) Discovery of potent pteridine reductase inhibitors to guide antiparasite drug development. *Proc. Natl. Acad. Sci. U.S.A.* 105, 1448–1453.
- (14) Yuvaniyama, J., Chitnumsub, P., Kamchonwongpaisan, S., Vanichtanankul, J., Sirawaraporn, W., Taylor, P., Walkinshaw, M. D., and Yuthavong, Y. (2003) Insights into antifolate resistance from malarial DHFR-TS structures. *Nat. Struct. Biol.* 10, 357–365.
- (15) Knighton, D. R., Kan, C. C., Howland, E., Janson, C. A., Hostomska, Z., Welsh, K. M., and Matthews, D. A. (1994) Structure of and kinetic channelling in bifunctional dihydrofolate reductase-thymidylate synthase. *Nat. Struct. Biol.* 1, 186–194.
- (16) Senkovich, O., Schormann, N., and Chattopadhyay, D. (2009) Structures of dihydrofolate reductase-thymidylate synthase of *Trypanosoma cruzi* in the folate-free state and in complex with two antifolate drugs, trimetrexate and methotrexate. *Acta Crystallogr., Sect. D: Biol. Crystallogr.* 65, 704–716.
- (17) Chitnumsub, P., Yuvaniyama, J., Chahomchuen, T., Vilaivan, T., and Yuthavong, Y. (2009) Crystallization and preliminary crystallographic studies of dihydrofolate reductase-thymidylate synthase from *Trypanosoma cruzi*, the Chagas disease pathogen. *Acta Crystallogr., Sect. F: Struct. Biol. Cryst. Commun.* 65, 1175–1178.
- (18) O'Neil, R. H., Lilien, R. H., Donald, B. R., Stroud, R. M., and Anderson, A. C. (2003) Phylogenetic classification of protozoa based on the structure of the linker domain in the bifunctional enzyme, dihydrofolate reductase-thymidylate synthase. *J. Biol. Chem.* 278, 52980–52987.
- (19) Kongsaeree, P., Khongsuk, P., Leartsakulpanich, U., Chitnumsub, P., Tarnchompoo, B., Walkinshaw, M. D., and Yuthavong, Y. (2005) Crystal structure of dihydrofolate reductase from *Plasmodium vivax*: pyrimethamine displacement linked with mutation-induced resistance. *Proc. Natl. Acad. Sci. U.S.A.* 102, 13046–13051.
- (20) Sirawaraporn, W., Sathitkul, T., Sirawaraporn, R., Yuthavong, Y., and Santi, D. V. (1997) Antifolate-resistant mutants of *Plasmodium falciparum* dihydrofolate reductase. *Proc. Natl. Acad. Sci. U.S.A.* 94, 1124–1129.
- (21) Sawaya, M. R., and Kraut, J. (1997) Loop and subdomain movements in the mechanism of *Escherichia coli* dihydrofolate reductase: crystallographic evidence. *Biochemistry* 36, 586–603.
- (22) Kamchonwongpaisan, S., Quarrell, R., Charoensetakul, N., Ponsinet, R., Vilaivan, T., Vanichtanankul, J., Tarnchompoo, B., Sirawaraporn, W., Lowe, G., and Yuthavong, Y. (2004) Inhibitors of multiple mutants of *Plasmodium falciparum* dihydrofolate reductase and their antimalarial activities. *J. Med. Chem.* 47, 673–680.
- (23) Chitnumsub, P., Yuvaniyama, J., Vanichtanankul, J., Kamchonwongpaisan, S., Walkinshaw, M. D., and Yuthavong, Y. (2004) Characterization, crystallization and preliminary X-ray analysis of bifunctional dihydrofolate reductase-thymidylate synthase from *Plasmodium falciparum*. *Acta Crystallogr., Sect. D: Biol. Crystallogr.* 60, 780–783.
- (24) Gamarro, F., Yu, P. L., Zhao, J., Edman, U., Greene, P. J., and Santi, D. (1995) *Trypanosoma brucei* dihydrofolate reductase-thymidylate synthase: gene isolation and expression and characterization of the enzyme. *Mol. Biochem. Parasitol.* 72, 11–22.
- (25) Bradford, M. M. (1976) A rapid and sensitive method for the quantitation of microgram quantities of protein utilizing the principle of protein-dye binding. *Anal. Biochem.* 72, 248–254.
- (26) Hillcoat, B. L., Nixon, P. F., and Blakley, R. L. (1967) Effect of substrate decomposition on the spectrophotometric assay of dihydrofolate reductase. *Anal. Biochem.* 21, 178–189.
- (27) Jenson, N. P., Ager, A. L., Bliss, R. A., Canfield, C. J., Kotecka, B. M., Rieckmann, K. H., Terpinski, J., Jacobus, D. P. (2001) Phenoxypropoxybiguanides, prodrugs of DHFR-inhibiting diaminotriazine antimicrobials. *J. Med. Chem.* 44, 3925–3931.
- (28) Gros, L., Castillo-Acosta, V. M., Jimenez Jimenez, C., Sealey-Cardona, M., Vargas, S., Manuel Estevez, A., Yardley, V., Rattray, L., Croft, S. L., Ruiz-Perez, L. M., Urbina, J. A., Gilbert, I. H., and Gonzalez-Pacanowska, D. (2006) New azasterols against *Trypanosoma brucei*: role of 24-sterol methyltransferase in inhibitor action. *Antimicrob. Agents Chemother.* 50, 2595–2601.
- (29) Hirumi, H., and Hirumi, K. (1989) Continuous cultivation of *Trypanosoma brucei* blood stream forms in a medium containing a low concentration of serum protein without feeder cell layers. *J. Parasitol.* 75, 985–989.
- (30) Chayen, N. E., Shaw Stewart, P. D., and Blow, D. M. (1992) Microbatch crystallization under oil—a new technique allowing many small-volume crystallization trials. *J. Cryst. Growth* 122, 176–180.
- (31) Otwinowski, Z., Minor, W., Charles W. Carter, Jr. (1997) Processing of X-ray diffraction data collected in oscillation mode, in *Methods in enzymology*, pp 307–326, Academic Press, New York.
- (32) Navaza, J. (1994) AMoRe: an automated package for molecular replacement. *Acta Crystallogr., Sect. A: Found. Crystallogr.* 50, 157–163.
- (33) (1994) The CCP4 suite: programs for protein crystallography, Collaborative Computational Project, Number 4, *Acta Crystallogr., Sect. D: Biol. Crystallogr.* 50, 760–763.
- (34) Brunger, A. T., Adams, P. D., Clore, G. M., DeLano, W. L., Gros, P., Grosse-Kunstleve, R. W., Jiang, J. S., Kuszewski, J., Nilges, M., Pannu, N. S., Read, R. J., Rice, L. M., Simonson, T., and Warren, G. L. (1998) Crystallography & NMR system: A new software suite for macromolecular structure determination. *Acta Crystallogr., Sect. D: Biol. Crystallogr.* 54, 905–921.
- (35) Jones, T. A., Zou, J. Y., Cowan, S. W., and Kjeldgaard, M. (1991) Improved methods for building protein models in electron density maps and the location of errors in these models. *Acta Crystallogr., Sect. A: Found. Crystallogr.* 47 (Pt 2), 110–119.
- (36) Laskowski, R. A., MacArthur, M. W., Sali, M. D., and Sali, T. J. (1993) PROCHECK: a program to check the stereochemical quality of protein structures. *J. Appl. Crystallogr.* 26, 283–291.
- (37) Schrodinger, L. L. C. (2010) The PyMOL Molecular Graphics System, Version 1.3r1.
- (38) Gouet, P., Courcelle, E., Stuart, D. I., and Metoz, F. (1999) ESPript: analysis of multiple sequence alignments in PostScript. *Bioinformatics* 15, 305–308.